Published in final edited form as:
J Neurosci. 2010 March 31; 30(13): 4757–4766. doi:10.1523/JNEUROSCI.6108-09.2010.

SAP102 is a highly mobile MAGUK in spines

Chan-Ying Zheng[1], **Ronald S. Petralia**[1], **Ya-Xian Wang**[1], **Bechara Kachar**[2], and **Robert J. Wenthold**[1,3]

[1] Laboratory of Neurochemistry, National Institute on Deafness and Other Communication Disorders, National Institutes of Health, Bethesda, Maryland 20892

[2] Laboratory of Cell Structure and Dynamics, National Institute on Deafness and Other Communication Disorders, National Institutes of Health, Bethesda, Maryland 20892

Abstract

Membrane associated guanylate kinases (MAGUKs), which are essential proteins in the postsynaptic density (PSD), cluster and anchor glutamate receptors and other proteins at synapses. The MAGUK family includes PSD-95, PSD-93, SAP102, and SAP97. Individual family members can compensate for one another in their ability to recruit and retain receptors at the postsynaptic membrane as shown through deletion and knockdown studies. SAP102 is highly expressed in both young and mature neurons, however, little is known about its localization and mobility at synapses. Here, we compared the distribution, mobility, and turnover times of SAP102 to the well-studied MAGUK, PSD-95. Using light and electron microscopy, we found that SAP102 shows a broader distribution as well as peak localization further away from the postsynaptic membrane than PSD-95. Using fluorescence recovery after photobleaching (FRAP), we found that 80% of SAP102 and 36% of PSD-95 are mobile in spines. Previous studies showed that PSD-95 was stabilized at the PSD by N-terminal palmitoylation. We found that stabilization of SAP102 at the PSD was dependent on its SH3/GK domains but not its PDZ interactions. Furthermore, we showed that stabilizing actin or blocking NMDA/AMPA receptors reduced the mobile pool of SAP102 but did not affect the mobile pool of PSD-95. Our results show significant differences in the localization, binding mechanism, and mobility of SAP102 and PSD-95. These differences and the compensatory properties of the MAGUKs point out an unrecognized versatility of the MAGUKs in their function in synaptic organization and plasticity.

Keywords

actin; postsynaptic; scaffolding proteins; synaptic transmission; glutamate receptor; trafficking

Introduction

Glutamate receptors are clustered at the postsynaptic membrane of excitatory synapses through interactions with a submembranous scaffolding complex known as the post synaptic density (PSD). This complex is made up of a number of interacting proteins with prominent members being the PSD-95 family of membrane associated guanylate kinases (MAGUKs), which include PSD-95, PSD-93, SAP102, and SAP97. The MAGUKs interact directly with NMDA receptors (Kornau et al., 1995; Muller et al., 1996) and indirectly with AMPA receptors through

Corresponding author: Correspondence should be addressed to Dr. Chan-Ying Zhengor Dr. Ronald S. Petralia, Laboratory of Neurochemistry, National Institute on Deafness and Other Communication Disorders, National Institutes of Health, Bethesda, Maryland 20892. zhengchan@nidcd.nih.gov, petralia@nidcd.nih.gov.
[3]deceased.

transmembrane AMPA receptor regulatory proteins (TARPs) (Nicoll et al., 2006). MAGUKs play critical roles in mediating synaptic plasticity by regulating synaptic glutamate receptors (Funke et al., 2005) and family members can compensate for one another in maintaining synaptic transmission. (Elias et al., 2006; Schluter et al., 2006). PSD-95 is highly clustered at postsynaptic sites and a number of studies have shown that both the clustering (El-Husseini et al., 2002) and delivery (El-Husseini et al., 2000b) of PSD-95 to the synapse associated with tubular-vesicular structures is dependent on palmitoylation of cysteine residues at positions 3 and 5. Under resting conditions, PSD-95 is relatively immobile while other PSD components, for example CaMKII, Shank, βSAP97, and GKAP are more mobile in spines (Kuriu et al., 2006; Sharma et al., 2006; Waites et al., 2009). However, recent studies have shown that synaptic activity can lead to a rapid turnover of PSD-95 in spines (Yoshii and Constantine-Paton, 2007; Steiner et al., 2008; Noritake et al., 2009).

While the role of PSD-95 in synaptic function has been extensively studied, the roles of the other MAGUKS are less certain (Elias and Nicoll, 2007). In particular, the role of SAP102 in postsynaptic organization and plasticity is unclear. SAP102 is highly expressed in neurons at the PSD as well as in dendrites and axons. In hippocampal neurons, it is abundantly expressed in young neurons and gradually decreases with maturation (Sans et al., 2000). PSD-95, on the other hand, is less expressed in young neurons and increases with maturation, suggesting that SAP102 may be particularly important during development. SAP102 lacks N-terminal cysteines and L27 domains that are required for synaptic clustering of PSD-95 and SAP97 (Nakagawa et al., 2004; Schluter et al., 2006), respectively, thus, raising the question of how SAP102 is enriched at the postsynaptic membrane.

In the present study we investigated the localization and mobility of SAP102 in spines and compared it to the well-characterized MAGUK, PSD-95. Using light and electron microscopy, we find that SAP102 and PSD-95 do not fully co-localize in spines. The SH3/GK domains but not the PDZ motifs are necessary for the enrichment of SAP102 in spines. Using fluorescence recovery after photobleaching (FRAP) analysis, we find that the majority of SAP102 in spines turns over within 5 minutes. Furthermore, the mobility of a portion of SAP102 in spines is dependent on actin and glutamate receptor activation. Our results demonstrate that SAP102 and PSD-95 are differentially localized and mobilized in spines; this may underlie functional differences between the two proteins in synaptic organization and plasticity.

Materials and Methods

DNA constructs

GFP-SAP102 and GFP-actin was described previously (Rzadzinska et al., 2004; Sans et al., 2005). GFP-PSD-95 and GFP-C3, 5S-PSD-95 were gifts from Dr. David S. Bredt (UCSF, San Francisco, CA); DsRed (pDsRed-Monomer-C1) was a gift from Dr. Zu-Hang Sheng (NIH, Bethesda, MD). GFP (pEGFP-N3) was purchased from Clontech, Mountain View, CA. GFP-SAP102ΔSH3GK, GFP-SAP102ΔSH3 and GFP-SAP102ΔGK were generated by mutating Y483 to a stopcodon (TAT to TAG), deleting the regions between 526A and 585V, and mutating E589 to a stopcodon (GAG to TAG), respectively. GFP-SAP102PDZ1FH encompassed the mutation 161 F →H, GFP-SAP102PDZ2FH had 256 F→H, and GFP-SAP102PDZ3FH had 416 F→H. Each of the three mutants abolishes the PDZ binding between a PDZ domain and the C-terminal carboxylate group of group1 PDZ ligands (Doyle et al., 1996; Regalado et al., 2006).

Antibodies

A mouse monoclonal antibody to PSD-95 was purchased from ABR (Rockford, IL; clone 7E3-1B8) and was used at 1:100 for immunofluorescence. A rabbit polyclonal antibody to

SAP102 (JH62514) was a gift from Johannes Hell and was used at 1:3000 for immunofluorescence. The PSD-95 antibody that was used for immunogold staining was from BD Bioscience (San Jose, CA). All of these antibodies were characterized and compared previously (Sans et al., 2000; Davies et al., 2001).

Immunofluorescence microscopy

All animal procedures were done in accordance with the National Institutes of Health Guide for the Care and Use of Laboratory Animals (NIH publication 85-23) under NIDCD protocol #1167-07. Hippocampal neurons were cultured on coverlips from E18 fetal rat hippocampus (Sans et al., 2001). The neurons were transfected on 17 days in vitro (DIV) using CalPhos Mammalian Transfection Kit (Clontech, Palo Alto, CA) (Sans et al., 2003). Three to four days later, neurons were fixed with a 1:1 mixture of methanol and acetone at −20°C for 4 minutes. Then on ice, neurons were washed with PBS, permeablilized in 0.25% Triton-X-100 for 5 minutes, blocked in PBS containing 10% normal goat serum (NGS) for 1 hour, incubated with primary antibody in PBS containing 3% NGS and 0.1% Triton-X-100 (N-T-PBS) for 1 hour, washed with PBS, incubated with FITC- or CY3- conjugated secondary antibody in N-T-PBS for 30 minutes, and then washed again with PBS. Finally, the coverslips were mounted using ProLong Gold Antifade reagent (Invitrogen, Carlsbad, CA), and imaged using an UltraVIEW ERS confocal Microscope (PerkinElmer, Fremont, CA). When labeled by SAP102 or PSD-95 antibody, the average immunofluorescence intensity of GFP-SAP102 or GFP-PSD-95 transfected neurons was estimated to be 2 times as bright as that of the non-transfected neighboring neurons.

Immunogold

Postembedding immunogold labeling was based on established methods (Petralia and Wenthold, 1999; Petralia et al., 2003; Petralia et al., 2005; Yi et al., 2007). Briefly, rats were perfused with 4% paraformaldehyde plus 0.5% glutaraldehyde, and sections were cryoprotected and frozen in a Leica EM CPC (Vienna, Austria), and further processed and embedded in Lowicryl HM-20 resin using a Leica AFS freeze-substitution instrument. Thin sections were incubated in 0.1% sodium borohydride+50 mM glycine/Tris-buffered saline + 0.1% Triton X-100 (TBST), followed by 10% NGS in TBST, and primary antibody in 1% NGS/TBST overnight, and then immunogold labeling in 1% NGS in TBST plus 0.5% polyethylene glycol (20,000 MW). Finally, sections were stained with uranyl acetate and lead citrate. For double labeling, the 2 primary antibodies were applied together and so were the 2 secondary antibodies. Corresponding controls, lacking the primary antibody, showed only rare gold labeling. Images were stored in their original formats and final images for figures were prepared in Adobe Photoshop: levels and brightness/contrast of images were minimally adjusted, evenly over the entire micrograph.

FRAP

Hippocampal neurons were cultured on poly-L-lysine coated glass-bottom dishes (MatTek, Ashland, MA) at E18, and then transfected on 16~18 DIV. Neurons were used for FRAP experiment 4 days after transfection. The culture medium was exchanged with pre-warmed Tyrode Solution before experiments. Tyrode Solution contained (in mM) NaCl 145, KCl 5, HEPES 10, Glucose 10, Glycine 0.005, $CaCl_2$ 2.6, and $MgCl_2$ 1.3 (pH adjusted to 7.4 with NaOH). Temperature was kept at 37°C using a Zeiss TempModule system. Depending on the experiments, 10 μM Jasplakinolide (EMD, La Jolla, CA), 100 μM DL-APV and 20 μM NBQX-disodium salt hydrate (Tocris, Ellisville, MO) were added into Tyrode Solution 30–60 minutes before FRAP recording and during FRAP recording. Control coverslips were incubated with prewarmed Tyrode Solution or 1% DMSO instead of the drugs.

All images were captured using a Zeiss LSM510 confocal microscope with a 100x objective, using 5x optical zoom and a 256×256 pixel resolution. The pinhole was set to 1000 and the 488 laser output was 70%. Spines of interest were bleached 10 times at 100% laser transmission. These conditions are sufficient to bleach the fluorescence of a spine to background level in a fixed preparation. During our FRAP measurements, we used speed 9 which took 0.5 second to finish a scan. A series of images was captured before and immediately after photobleaching with 3% laser transmission. Five images were captured before bleaching; their average fluorescence intensity was set to 100%. For most experiments, images were captured every 3 sec for the first minute after bleaching, and then at 2, 3, 4, 5, 10, 15 and 20 minutes.

ImageJ software (NIH, Bethesda, MD) was used for aligning the images and measuring fluorescence intensity of the region of interest in time-lapse photography. For each movie, the mean intensity of an untransfected area was measured as background and was subtracted from the original intensity. Graphpad Prism software (Graphpad software, La Jolla, CA) was used for curve fitting.

We divided the total fluorescence of spine proteins into the immobile fraction (f_i) and the mobile fraction (f_m). The mobile fraction was divided into a slow mobile fraction (f_s) and a rapid mobile fraction (f_r)(Star et al., 2002).

$$1=f_i+f_m=f_i+f_s+f_r \quad (1)$$

The immobile fraction is:

$$f_i=1-f_m \quad (2)$$

The mobile fraction of the spines is described as:

$$f_m=(F_\infty - F_b)/(F_0 - F_b) \quad (3)$$

where F_∞ represents the fluorescence of region of interest after full recovery from bleaching, F_b represents the background fluorescence intensity, and F_0 is the mean fluorescence before bleaching.

The slow mobile fraction is reflected by FRAP during a 20 minute period, curve fit by one-phase exponential equations:

$$y=a^*\exp(-bx) \quad (4)$$

The rapid mobile fractions were detected immediately after photobleaching. According to equation (1) they could be given by the equation:

$$f_r=1-f_i-f_s \quad (5)$$

The half recovery time ($\tau_{1/2}$) of the rapid fraction was calculated by Graphpad Prime software, using the total binding model.

The half recovery time of a freely diffusing protein in spines is calculated by comparing the target protein to pEGFP. pEGFP, which is presumable to be freely diffusing in the cytoplasm,

had a $\tau_{1/2}$ =0.9 seconds in our system. $\tau_{1/2}$ is related to the cube root of the protein size (Star et al., 2002). Therefore, free diffusion of GFP-SAP102 and GFP-PSD-95 both would have a $\tau_{1/2}$ = 1.4 seconds, since they had similar molecular weights of 113 and 109 kD. $\tau_{1/2}$ of the free diffusional GFP-SAP102ΔSH3GK (80 kD) would be 1.2 second in our system.

Data analysis

The immunochemistry data were analyzed using MetaMorph software (Universal Imaging Corporation, West Chester, PA). For spine/dendrite ratio analysis, mushroom spines of secondary dendrites and adjacent dendrite shaft regions were defined under the DsRed channel. Then under the GFP channel, the regions of interest were reloaded. The mean intensity of GFP tagged protein in spine regions and dendrite regions was measured. In each neuron, a minimum number of 10 pairs of spines and adjacent dendrite regions from at least 2 dendrites were used for determining a mean spine/dendrite ratio. In total, 5–15 pyramidal neurons from 2–3 parallel transfections were analyzed. Statistical significance between two data sets was calculated using a Student's t-test.

The perpendicular distance from the center of immunogold particle to the postsynaptic membrane was measured using ImageJ software. The distribution of the gold particles was analyzed by IGOR pro software (WaveMetrics, Portland, OR). Gold particles were included that were completely or partially over the synapse. The gold particles between pre- and post-synaptic membrane were given a negative number. Presynaptic particles were not included.

Results

SAP102 and PSD-95 are differentially distributed in spines

Previous studies have shown that PSD-95 is mainly enriched at postsynaptic sites while SAP102 is present in dendrites, axons, as well as postsynaptic sites (El-Husseini et al., 2000c; Sans et al., 2005). To compare the distributions of SAP102 and PSD-95 in cultured hippocampal neurons, we first examined the enrichment of both proteins in spines relative to dendrites by measuring the mean fluorescence intensity of immunolabeling of endogenous SAP102 and PSD-95 in spines and adjacent dendrites. Neurons were fixed and labeled at 21 days in vitro (DIV) (Fig. 1*A*). The fluorescence ratio for SAP102 in spines compared to dendrites was 2.0 ± 0.4 while for PSD-95 it was 5.4 ± 0.9, confirming that, while both are enriched in spines, PSD-95 is relatively more concentrated than SAP102. These ratios were similar to those from neurons transfected with GFP-SAP102 or GFP-PSD-95. The spine/dendrite ratio of GFP-SAP102 expressing neurons was 2.5 ± 0.6 and that of GFP- PSD-95 expressing neurons was 6.2 ± 1.0. We further studied the distributions of SAP102 and PSD-95 in spines by double labeling 21 DIV neurons using antibodies selective for SAP102 and for PSD-95 (Sans et al., 2000). While both were enriched in spines, the extensive overlap between SAP102 and PSD-95 was more obvious when viewed with high magnification imaging using a Yokogawa spinning disk confocal microscope (Fig. 1*B*). A plot of the fluorescence intensity profile for the green and red channels showed that the peak fluorescence of endogenous SAP102 and PSD-95 largely overlapped, while the SAP102 had a broader distribution than that of PSD-95. Further, the fluorescence peak of SAP102 was consistently slightly shifted away from that of PSD-95 (Fig. 1*B, C*, more examples in supplementary Fig. 1), indicating that SAP102 and PSD-95 did not cluster in the identical micro areas in the same spine. To investigate this in more detail, we carried out immunogold labeling of SAP102 or PSD-95 in the CA1 stratum radiatum of postnatal day 37 (P 37) rat hippocampus, and measured the perpendicular distance of the gold particles from the postsynaptic membrane of the spines (Fig. 1*D, E*). As defined by previous studies (Valtschanoff and Weinberg, 2001), the PSD lies predominantly within the first 50 nm from the postsynaptic membrane. The distribution map showed similar localization patterns for SAP102 and PSD-95. Both SAP102 and PSD-95 were

concentrated in the PSD area (69.4% of SAP102 and 94.2% of PSD-95), although the median value of PSD-95 was 10 nm closer to the postsynaptic membrane than SAP102 (13.5 nm for PSD-95, 24.2 nm for SAP102). Being consistent with light microscope observation, SAP102 had a wider distribution in the region of the cytoplasm than PSD-95: 30.6% of SAP102 (n = 144) and 5.8% of PSD-95 (n = 192) was located between 50 nm and 500 nm from the postsynaptic membrane. Double labeling immunogold showed an indistinguishable distribution from that obtained with single labeling. Using double labeling immunogold, the percentage of gold particles between 50 and 500 nm from the postsynaptic membrane was 30.2% (n = 102) and 6.9% (n = 139) for SAP102 and PSD-95, respectively. In addition to their localization in spines, both SAP102 and PSD-95 were also present in dendrites, presumably associated with transport vesicles (El-Husseini et al., 2000b). Analysis of immunoreactivity in dendrites in double stained neurons showed little colocalization (supplementary Fig. 2).

SAP102 has a larger mobile fraction than PSD-95 in spines

Previous studies showed that almost half of the PSD-95 was immobile in the spine for up to 60 minutes (Kuriu et al., 2006; Sharma et al., 2006; Steiner et al., 2008). To compare the mobilities of SAP102 and PSD-95 in spines, we expressed GFP-SAP102 or GFP-PSD-95 in cultured hippocampal neurons, and then measured FRAP 3–4 days later (Fig. 2*A–D* and supplementary Movie 1, 2). The recovery of fluorescence in spines during a 20 minute time course was divided into three components: the immobile fraction, the slow mobile fraction and the rapid mobile fraction (Star et al., 2002; Sprague and McNally, 2005). The mobile fraction, which equals the sum of slow and rapid mobile fractions, was the total fluorescence recovered in 20 minutes. The mobile fractions of GFP-SAP102 and GFP-PSD-95 were 80.5 ± 10.2% and 36.2 ± 9.3%, respectively (Fig. 2*E*), showing that SAP102 has a larger mobile fraction than PSD-95 in spines.

The mobile fractions of GFP-SAP102 and GFP-PSD-95 had similar fluorescence recovery patterns (Fig. 2*C–D*); both recoveries were rapid in the first 10 seconds and then slowed until reaching their maximal recovery levels in minutes. GFP-SAP102 and GFP-PSD-95 had rapid mobile components with half recovery times ($\tau_{1/2}$) of 1.5 ± 0.3 and 0.5 ± 0.2 seconds, whereas the slow mobile components had $\tau_{1/2}$ of 44.4 ± 8.4 and 46.2 ± 11.7 seconds, respectively. The slow mobile components were defined by FRAP curves, which matched one-phase exponential equations from 10 seconds to minutes (see SI methods for detail). 58.1 ± 8.0% of total GFP-SAP102 and 24.4 ± 4.0% of total GFP-PSD-95 in spines was present in the slow mobile fractions (Fig. 2*F*). The rapid mobile fractions for GFP-SAP102 and GFP-PSD-95 were 22.4 ± 3.7% and 11.7 ± 3.6%, respectively.

SH3/GK domains are required for SAP102 enrichment and stabilization in spines

SAP102 lacks the N-terminal cysteine palmitoylation sites, which mediate the synaptic clustering of PSD-95 (supplementary Fig. 3A–B) (Schluter et al., 2006), although a previous study suggested that the N-terminus of SAP102 may play a role through a non-palmitoylation mechanism (Firestein et al., 2000). To determine if the PDZ or SH3/GK domains are important for clustering SAP102 in spines, we deleted the SH3/GK domains by inserting a stop codon immediately after PDZ3 of GFP-SAP102 (GFP-SAP102ΔSH3GK). Neurons expressing GFP-SAP102ΔSH3GK were fluorescent throughout the cell, including cell body, dendrite, spine and axon. However, their spine fluorescence enrichment was decreased dramatically compared to that of GFP-SAP102. Spine enrichment was quantified by determining spine/dendrite fluorescence ratios of GFP, GFP-SAP102ΔSH3GK, and GFP-SAP102 (Fig. 3A). Neurons were co-transfected with DsRed to define spine and adjacent dendrite shaft regions. The spine/dendrite green fluorescence ratio of GFP-SAP102ΔSH3GK was 1.1 ± 0.3, close to the ratio of the GFP vector control (0.9 ± 0.1; Fig. 3B), and significantly smaller than that of GFP-PSD-95ΔSH3GK (2.2 ± 0.4, $p<0.05$; supplementary Fig. 3C). The ratio for GFP-SAP102 was

2.5 ± 0.6. Furthermore, we measured the neurons expressing GFP-SAP102 mutations that lack either SH3 or GK domains. The spine/dendrite green fluorescence ratios of GFP-SAP102ΔSH3 and GFP-SAP102ΔGK were 2.4 ± 0.3 and 1.6 ± 0.3, respectively. On the other hand, expression of mutants that abolish each individual PDZ domains did not affect significantly the clustering of SAP102 in spines (Fig. 3A–B). The spine/dendrite green fluorescence ratios were 2.4 ± 0.5, 2.3 ± 0.2 and 2.5 ± 0.8 for GFP-SAP102PDZ1FH, GFP-SAP102PDZ2FH and GFP-SAP102PDZ3FH, respectively. All together the data above suggest that SH3/GK domains are required for SAP102 clustering in spines, while the single PDZ mutations have no influence in the clustering.

We next investigated the role of the SH3/GK domains in the mobility of SAP102 in spines. We transfected neurons with GFP, GFP-SAP102 or GFP-SAP102ΔSH3GK, and then performed FRAP analysis in spines (Fig. 4A–C). As we expected, GFP-SAP102ΔSH3GK recovered rapidly after photobleaching with a $\tau_{1/2}$=1.2 second, similar to that of GFP (0.9 second), and dramatically shorter than that of GFP-SAP102 (Fig. 4D–E). The slow mobile fraction was not detected in the FRAP of GFP-SAP102ΔSH3GK, thus, the movement of GFP-SAP102ΔSH3GK in spines is likely due to free diffusion, suggesting the SH3/GK domains are necessary for SAP102 stabilization in spines. On the other hand, the PDZ mutants had similar recovery patterns as GFP-SAP102. The total half recovery times for GFP-SAP102, GFP-SAP102PDZ1FH, GFP-SAP102PDZ2FH and GFP-SAP102PDZ3FH were 33.4 ± 6.7, 33.5 ± 10.8, 35.5 ± 6.0 and 29.8 ± 5.9 seconds, respectively (Fig. 4E), suggesting that single PDZ mutation does not influence the turnover rate of SAP102 in spines.

SAP102 mobility depends on actin dynamics

It has been shown that the SH3/GK domains of the MAGUKs are indirectly linked to actin through proteins of the PSD including GKAP and SPAR (Naisbitt et al., 2000; Pak et al., 2001; Gerrow et al., 2006). Turnover of actin associated proteins, for example GKAP, depends on actin turnover (Kuriu et al., 2006). To investigate whether actin dynamics play a role in the mobility of SAP102 in spines, we incubated GFP-actin, GFP-SAP102 and GFP-PSD-95 transfected neurons with an actin-stabilizing drug, Jasplakinolide, for 20 minutes, and then performed FRAP (Fig. 5*A*–*F*). Jasplakinolide is a potent inducer of actin stabilization, and has been shown previously to block actin turnover in spines (Star et al., 2002); therefore, any recovery that depends on the turnover of actin will be inhibited by the presence of Jasplakinolide. As expected, Jasplakinolide treatment produced a block of GFP-actin turnover in spines (Fig. 5*D*). Jasplakinolide treatment increased the immobile fraction of GFP-SAP102 to 40.4 ± 9.4%, compared to 23.6 ± 8.9% in DMSO control, while it decreased the slow mobile fraction to 51.3 ± 15.9%, compared to 67.7 ± 12.5% in control spines (Fig. 5*E*, *G*). The change in the rapid mobile fraction was not significant. However, stabilizing actin does not have an effect on GFP-PSD-95 (Fig. 5*F*, *H*). After Jasplakinolide treatment, the immobile, slow mobile and rapid mobile fractions of total GFP-PSD-95 in spines were 74.8 ± 7.8%, 16.8 ± 6.0% and 8.4 ± 5.8%, respectively, compared to DMSO control values of 68.6 ± 7.2%, 20.8 ± 8.9% and 10.5 ± 4.2%, respectively. These data show that the mobility of spine GFP-SAP102 is partly actin-dependent while mobility of GFP-PSD-95 is largely independent of actin.

SAP102 and PSD-95 are independently regulated in spines

All four MAGUKs are concentrated at the PSD and interact with a multitude of binding partners at the synaptic membrane, including direct interactions with NMDA receptors and indirect interactions with AMPA receptors. An important question, therefore, is whether SAP102 and PSD-95 are independently regulated in spines. To address this, we asked if overexpression of PSD-95 or SAP102 changed the amount of endogenous SAP102 or PSD-95, respectively, in spines. Endogenous SAP102 and PSD-95 in non-transfected neighboring neurons were used as a control. We found that overexpression of SAP102 did not change endogenous spine

PSD-95 level (supplementary Fig. 4*A–C*) and similarly, that overexpression of PSD-95 had no effect on endogenous spine SAP102 level (supplementary Fig. 4*D–E*). Next we asked if blockade of NMDA and AMPA receptors changed the mobility of GFP-SAP102 and GFP-PSD-95 in spines. We incubated GFP-SAP102 or GFP-PSD-95 transfected neurons with the NMDA receptor antagonist DL-APV (100 μM) and AMPA receptor antagonist DNQX (20 μM) for 1 hour, and then performed FRAP. The acute blockade of NMDA and AMPA receptors did not affect actin turnover (supplementary Fig. 5), however the mobile fraction of spine GFP-SAP102 was significantly decreased to 52.5 ± 17.3%, compared to the control value of 77.7 ± 6.2% (Fig. 6*A–C*). The slow mobile fraction significantly decreased (45.0 ± 15.8% for drug treatment, and 70.5 ± 2.2% for control), while the change in the rapid mobile fraction was not significant (7.5 ± 1.9% for drug treatment, and 7.1 ± 5.1% for control). Our experiments showed that APV alone inhibited the half recovery time of SAP102 (supplementary Fig. 6A). Blockade of NMDA and AMPA receptors with or without the actin stabilizer Jasplakinolide produced a similar decrease in the mobility of SAP102 (supplementary Fig. 6B). On the other hand, blockade of NMDA and AMPA receptors did not lead to a significant change in the mobility of GFP-PSD-95 in spines (Fig. 6*D–F*). After APV and DNQX treatment, the immobile, slow mobile and rapid mobile fractions of total GFP-PSD-95 in spines were 68.3 ± 10.5%, 23.4 ± 8.8%, and 8.3 ± 4.0%, respectively, compared to control values of 66.2 ± 1.6%, 20.0 ± 10.0%, and 13.7 ± 9.1%, respectively. These results suggest that SAP102 and PSD-95 are individually regulated in spines under basal conditions and during acute blockade of NMDA and AMPA receptors. This is consistent with our observation that the two MAGUKs are concentrated in spines through distinct mechanisms.

Discussion

In this study, we analyzed the distribution and trafficking of SAP102 in spines. Although both SAP102 and PSD-95 are enriched in spines, SAP102 is expressed in both the PSD and throughout the cytoplasm in spines while PSD-95 is highly localized to the PSD. Unlike PSD-95, which requires its N-terminus for localization at the PSD, SAP102 requires its SH3/GK domains. FRAP recordings in spines of hippocampal neurons in vitro revealed a larger mobile fraction of GFP-SAP102 compared to that of GFP-PSD-95. Moreover, stabilization of actin or blockade of glutamate receptor activity partly blocked the turnover of GFP-SAP102 in spines, showing that the mobility of spine GFP-SAP102 is partly actin dependent while mobility of GFP-PSD-95 is largely independent of actin. Our results suggest that SAP102 and PSD-95 play different roles in the trafficking and organization of glutamate receptors at the synapse, and, therefore, have distinct roles in synaptic plasticity.

Distribution of SAP102 in spines

It has been shown that PSD-95 is mainly enriched at postsynaptic sites while SAP102 is present in dendrites, axonal growth cones, and mature axons, as well as in postsynaptic sites (El-Husseini et al., 2000c). In this study, we focused on the distribution of SAP102 and PSD-95 in spines. Our light microscope and EM data showed that the majority of endogenous PSD-95 and SAP102 is clustered at the PSD. According to our EM data, 94.2% of PSD-95 in the spine co-localizes with the PSD, while 69.4% of SAP102 co-localizes with the PSD. The greater association of PSD-95 with the postsynaptic membrane may be related to the different mechanisms by which the two MAGUKs are clustered. PSD-95 clustering at postsynaptic sites is dependent on palmitoylation of cysteine residues 3 and 5 at its N-terminus (supplementary Fig. 3) (Craven et al., 1999; El-Husseini et al., 2002). Studies showed that PSD-95 truncated after PDZ-2, which deleted PDZ3 and SH3/GK domains, still clustered in spines. In contrast, our studies showed that SAP102 lacking the SH3/GK or GK domain has no or only minor clustering in spines (Fig. 3), suggesting that there are different mechanisms by which SAP102 and PSD-95 are enriched in spines. Some studies have shown that PSD-95 lacking the SH3/

GK domains fails to cluster with knock-down of endogenous PSD-95, suggesting that truncated PSD-95 forms dimers with endogenous PSD-95 through their N-termini (Steiner et al., 2008; Xu et al., 2008). Unlike PSD-95, we find that expression of SAP102 in heterologous cells does not lead to the formation of dimers, indicating another major difference between the two MAGUKs (unpublished data). One possibility is that SAP102 associates with other PSD components via other proteins that bind to its GK domain. GK binding proteins, including GKAP, SPAR, BEGAIN, and MAP1A, are present in the PSD (Lim et al., 2003). GKAP, for example, interacts with GK domains of all four MAGUKs, and promotes clustering of PSD-95 and NMDA receptors (Kim et al., 1997). Knockdown of PSD-95 leads to a reduction of GKAP puncta in neurons (Gerrow et al., 2006). Future studies may be able to better delineate these interactions.

The mobility of SAP102 in spines

We defined two populations of PSD-95 and SAP102 in spines: an immobile fraction that does not recover within 20 minutes after photobleaching, and a mobile fraction that recovers within 20 minutes after photobleaching. We further divided the mobile fraction into slow mobile and rapid mobile fractions. The rapid mobile fraction likely represents molecules undergoing free diffusion since the $\tau_{1/2}$ of this fraction for both SAP102 and PSD-95 is similar to that of GFP alone, while the slow mobile fraction, with $\tau_{1/2}$ of about 45 seconds, likely represents a weak or transient interaction with other proteins of the PSD. A major difference between PSD-95 and SAP102 is their relative amounts associated with mobile and immobile fractions. The majority of PSD-95 is immobile (63.8%) while the majority of SAP102 is mobile (80.5%). The large immobile pool of PSD-95 may be due to its association with the plasma membrane through N-terminal palmitoylation sites. SAP102 is stabilized through interactions involving its SH3/GK domains, and strong interactions with other stable proteins would be responsible for its immobile pool.

Our data showed that blocking the turnover of actin leads to a decrease of the mobile fraction of SAP102, suggesting that the mobility of SAP102 is partly mediated by actin. Actin is a core skeletal component in spines; it interacts with multiple PSD proteins (Engqvist-Goldstein and Drubin, 2003). MAGUKs bind indirectly to actin: SAP97 – MyosinVI – actin, PSD-95 – SPAR – actin, PSD-95 – GKAP – Shank – cortactin – actin, and PSD-95 – NMDAR – actinin – actin (Petralia et al., 2008). One model to explain the decrease of SAP102 mobile fraction after stabilizing actin is that the stability of SAP102 may be determined by the stability of its interacting partners. The immobile and mobile pools of proteins that associate with SH3/GK domains of MAGUKS, such as GKAP and Shank, have been characterized (Kuriu et al., 2006; Sharma et al., 2006). The mobile fraction of GKAP and Shank in spines also decreases after inhibiting the dynamics of actin (Kuriu et al., 2006), suggesting that the molecular mobility may reflect the current complex formed or due to the population of interacting molecules. Although PSD-95 also interacts with actin, our data are consistent with previous reports (Blanpied et al., 2008) showing that the stability of PSD-95 is not affected by the turnover rate of actin. One explanation is that PSD-95 forms a strong association with a group of proteins in the PSD and these interactions are stronger than the actin association. This hypothesis is consistent with the finding that PSD-95 remains clustered when both the actin and membrane are destroyed (Allison et al., 1998).

The role of SAP102 in receptor trafficking

Like PSD-95, SAP102 binds directly to NMDA receptors through the NR2 subunits (Lau et al., 1996; Al-Hallaq et al., 2007). The association of SAP102 with AMPA receptors through TARPs and its role in synaptic plasticity is less clear (Dakoji et al., 2003; Ives et al., 2004). Although PSD-95 is present in a large stoichiometric excess of glutamate receptors in the PSD (Chen et al., 2005), PSD-95 over-expression leads to an increase in synaptic PSD-95 (Schnell

et al., 2002) resulting in an increase in the number of synaptic AMPA receptors (El-Husseini et al., 2000a; Stein et al., 2003). One possible explanation is the PSD-95 is displacing other MAGUKs such as SAP102.

Previous data showed that over-expression of SAP102 only slightly increases AMPA receptor EPSCs (compared to a substantial enhancement with PSD-95 expression (Schnell et al., 2002)), and knockdown of SAP102 does not affect AMPA transmission. However, knockdown of SAP102 in PSD-93/PSD-95 knock-out animals significantly reduces the remaining AMPA receptor current, suggesting that SAP102 can compensate for PSD-95 and PSD-93 (Elias et al., 2006). Our data showed that while both SAP102 and PSD-95 are present at the PSD, they are regulated independently and are secured through different mechanisms. Blockade of glutamate receptors decreased both half recovery time and the amount of SAP102 in the mobile fraction. In contract, blockade of glutamate receptors did not change the mobility of PSD-95. SAP102 is secured to the PSD through the SH3/GK domains while PSD-95 requires its N-terminus. As noted above, the N-terminal link of PSD-95 to the plasma membrane may explain its large immobile pool, relative to that of SAP102. One model that fits the localization and mobility results is that SAP102 plays a role in the delivery of NMDA receptors to the plasma membrane, while PSD-95 (and PSD-93) secures receptors to the postsynaptic membrane. This model is consistent with earlier results showing that SAP102 associates with NMDA receptors early in the biosynthetic pathway and co-localizes with NMDA receptors on transport vesicles in dendrites (Washbourne et al., 2004; Sans et al., 2005). Since both PSD-95 and PSD-93 can be knocked out without affecting viability of the animals, SAP102 can compensate functionally. Our current results showing that SAP102 and PSD-95 are not co-localized in dendrites, and showing a large mobile pool of SAP102, are consistent with these two MAGUKs being associated with different populations of transport mechanisms. Since it can substitute for PSD-95 and PSD-93 and is the predominant MAGUK early in development, SAP102 also plays a role in signal transduction and anchoring receptors at synapses, and this could be associated with its immobile pool. Such a model requires an exchange between SAP102 and PSD-95, and since SAP102 is present at the PSD, a receptor/SAP102 complex could be delivered to synapses. It remains to be resolved whether or not this could be added directly to the postsynaptic membrane or elsewhere to the spine or dendrite. The fact that synaptic glutamate receptors are associated with different MAGUKs at synapses raises the interesting possibility that receptors may have different signaling properties depending on their associated MAGUK. The recent study (Atasoy et al., 2008) showing that different populations of NMDA receptors are activated by evoked and spontaneous glutamate release suggests that there are microdomains within synapses that could be organized based on the MAGUK with which the receptor is organized.

Supplementary Material

Refer to Web version on PubMed Central for supplementary material.

Acknowledgments

This work was supported by the National Institute on Deafness and Other Communication Disorders Intramural Program.

References

Al-Hallaq RA, Conrads TP, Veenstra TD, Wenthold RJ. NMDA di-heteromeric receptor populations and associated proteins in rat hippocampus. J Neurosci 2007;27:8334–8343. [PubMed: 17670980]

Allison DW, Gelfand VI, Spector I, Craig AM. Role of actin in anchoring postsynaptic receptors in cultured hippocampal neurons: differential attachment of NMDA versus AMPA receptors. J Neurosci 1998;18:2423–2436. [PubMed: 9502803]

Atasoy D, Ertunc M, Moulder KL, Blackwell J, Chung C, Su J, Kavalali ET. Spontaneous and evoked glutamate release activates two populations of NMDA receptors with limited overlap. J Neurosci 2008;28:10151–10166. [PubMed: 18829973]

Blanpied TA, Kerr JM, Ehlers MD. Structural plasticity with preserved topology in the postsynaptic protein network. Proc Natl Acad Sci U S A 2008;105:12587–12592. [PubMed: 18723686]

Chen X, Vinade L, Leapman RD, Petersen JD, Nakagawa T, Phillips TM, Sheng M, Reese TS. Mass of the postsynaptic density and enumeration of three key molecules. Proc Natl Acad Sci U S A 2005;102:11551–11556. [PubMed: 16061821]

Craven SE, El-Husseini AE, Bredt DS. Synaptic targeting of the postsynaptic density protein PSD-95 mediated by lipid and protein motifs. Neuron 1999;22:497–509. [PubMed: 10197530]

Dakoji S, Tomita S, Karimzadegan S, Nicoll RA, Bredt DS. Interaction of transmembrane AMPA receptor regulatory proteins with multiple membrane associated guanylate kinases. Neuropharmacology 2003;45:849–856. [PubMed: 14529722]

Davies C, Tingley D, Kachar B, Wenthold RJ, Petralia RS. Distribution of members of the PSD-95 family of MAGUK proteins at the synaptic region of inner and outer hair cells of the guinea pig cochlea. Synapse 2001;40:258–268. [PubMed: 11309841]

Doyle DA, Lee A, Lewis J, Kim E, Sheng M, MacKinnon R. Crystal structures of a complexed and peptide-free membrane protein-binding domain: molecular basis of peptide recognition by PDZ. Cell 1996;85:1067–1076. [PubMed: 8674113]

El-Husseini AE, Schnell E, Chetkovich DM, Nicoll RA, Bredt DS. PSD-95 involvement in maturation of excitatory synapses. Science 2000a;290:1364–1368. [PubMed: 11082065]

El-Husseini AE, Craven SE, Chetkovich DM, Firestein BL, Schnell E, Aoki C, Bredt DS. Dual palmitoylation of PSD-95 mediates its vesiculotubular sorting, postsynaptic targeting, and ion channel clustering. J Cell Biol 2000b;148:159–172. [PubMed: 10629226]

El-Husseini AE, Topinka JR, Lehrer-Graiwer JE, Firestein BL, Craven SE, Aoki C, Bredt DS. Ion channel clustering by membrane-associated guanylate kinases. Differential regulation by N-terminal lipid and metal binding motifs. J Biol Chem 2000c;275:23904–23910. [PubMed: 10779526]

El-Husseini AE, Schnell E, Dakoji S, Sweeney N, Zhou Q, Prange O, Gauthier-Campbell C, Aguilera-Moreno A, Nicoll RA, Bredt DS. Synaptic strength regulated by palmitate cycling on PSD-95. Cell 2002;108:849–863. [PubMed: 11955437]

Elias GM, Nicoll RA. Synaptic trafficking of glutamate receptors by MAGUK scaffolding proteins. Trends Cell Biol 2007;17:343–352. [PubMed: 17644382]

Elias GM, Funke L, Stein V, Grant SG, Bredt DS, Nicoll RA. Synapse-specific and developmentally regulated targeting of AMPA receptors by a family of MAGUK scaffolding proteins. Neuron 2006;52:307–320. [PubMed: 17046693]

Engqvist-Goldstein AE, Drubin DG. Actin assembly and endocytosis: from yeast to mammals. Annu Rev Cell Dev Biol 2003;19:287–332. [PubMed: 14570572]

Firestein BL, Craven SE, Bredt DS. Postsynaptic targeting of MAGUKs mediated by distinct N-terminal domains. Neuroreport 2000;11:3479–3484. [PubMed: 11095503]

Funke L, Dakoji S, Bredt DS. Membrane-associated guanylate kinases regulate adhesion and plasticity at cell junctions. Annu Rev Biochem 2005;74:219–245. [PubMed: 15952887]

Gerrow K, Romorini S, Nabi SM, Colicos MA, Sala C, El-Husseini A. A preformed complex of postsynaptic proteins is involved in excitatory synapse development. Neuron 2006;49:547–562. [PubMed: 16476664]

Ives JH, Fung S, Tiwari P, Payne HL, Thompson CL. Microtubule-associated protein light chain 2 is a stargazin-AMPA receptor complex-interacting protein in vivo. J Biol Chem 2004;279:31002–31009. [PubMed: 15136571]

Kim E, Naisbitt S, Hsueh YP, Rao A, Rothschild A, Craig AM, Sheng M. GKAP, a novel synaptic protein that interacts with the guanylate kinase-like domain of the PSD-95/SAP90 family of channel clustering molecules. J Cell Biol 1997;136:669–678. [PubMed: 9024696]

Kornau HC, Schenker LT, Kennedy MB, Seeburg PH. Domain interaction between NMDA receptor subunits and the postsynaptic density protein PSD-95. Science 1995;269:1737–1740. [PubMed: 7569905]

Kuriu T, Inoue A, Bito H, Sobue K, Okabe S. Differential control of postsynaptic density scaffolds via actin-dependent and -independent mechanisms. J Neurosci 2006;26:7693–7706. [PubMed: 16855097]

Lau LF, Mammen A, Ehlers MD, Kindler S, Chung WJ, Garner CC, Huganir RL. Interaction of the N-methyl-D-aspartate receptor complex with a novel synapse-associated protein, SAP102. J Biol Chem 1996;271:21622–21628. [PubMed: 8702950]

Lim IA, Merrill MA, Chen Y, Hell JW. Disruption of the NMDA receptor-PSD-95 interaction in hippocampal neurons with no obvious physiological short-term effect. Neuropharmacology 2003;45:738–754. [PubMed: 14529713]

Muller BM, Kistner U, Kindler S, Chung WJ, Kuhlendahl S, Fenster SD, Lau LF, Veh RW, Huganir RL, Gundelfinger ED, Garner CC. SAP102, a novel postsynaptic protein that interacts with NMDA receptor complexes in vivo. Neuron 1996;17:255–265. [PubMed: 8780649]

Naisbitt S, Valtschanoff J, Allison DW, Sala C, Kim E, Craig AM, Weinberg RJ, Sheng M. Interaction of the postsynaptic density-95/guanylate kinase domain-associated protein complex with a light chain of myosin-V and dynein. J Neurosci 2000;20:4524–4534. [PubMed: 10844022]

Nakagawa T, Futai K, Lashuel HA, Lo I, Okamoto K, Walz T, Hayashi Y, Sheng M. Quaternary structure, protein dynamics, and synaptic function of SAP97 controlled by L27 domain interactions. Neuron 2004;44:453–467. [PubMed: 15504326]

Nicoll RA, Tomita S, Bredt DS. Auxiliary subunits assist AMPA-type glutamate receptors. Science 2006;311:1253–1256. [PubMed: 16513974]

Noritake J, Fukata Y, Iwanaga T, Hosomi N, Tsutsumi R, Matsuda N, Tani H, Iwanari H, Mochizuki Y, Kodama T, Matsuura Y, Bredt DS, Hamakubo T, Fukata M. Mobile DHHC palmitoylating enzyme mediates activity-sensitive synaptic targeting of PSD-95. J Cell Biol 2009;186:147–160. [PubMed: 19596852]

Pak DT, Yang S, Rudolph-Correia S, Kim E, Sheng M. Regulation of dendritic spine morphology by SPAR, a PSD-95-associated RapGAP. Neuron 2001;31:289–303. [PubMed: 11502259]

Petralia RS, Wenthold RJ. Immunocytochemistry of NMDA receptors. Methods Mol Biol 1999;128:73–92. [PubMed: 10320974]

Petralia RS, Wang YX, Wenthold RJ. Internalization at glutamatergic synapses during development. Eur J Neurosci 2003;18:3207–3217. [PubMed: 14686895]

Petralia, RS.; Al-Hallaq, RA.; Wenthold, RJ. trafficking and targeting of NMDA receptors. In: VanDongen, AM., editor. Biology of the NMDA Receptor. 1. Taylor and Francis Group; 2008. p. 149-200.

Petralia RS, Sans N, Wang YX, Wenthold RJ. Ontogeny of postsynaptic density proteins at glutamatergic synapses. Mol Cell Neurosci 2005;29:436–452. [PubMed: 15894489]

Regalado MP, Terry-Lorenzo RT, Waites CL, Garner CC, Malenka RC. Transsynaptic signaling by postsynaptic synapse-associated protein 97. J Neurosci 2006;26:2343–2357. [PubMed: 16495462]

Rzadzinska AK, Schneider ME, Davies C, Riordan GP, Kachar B. An actin molecular treadmill and myosins maintain stereocilia functional architecture and self-renewal. J Cell Biol 2004;164:887–897. [PubMed: 15024034]

Sans N, Petralia RS, Wang YX, Blahos J 2nd, Hell JW, Wenthold RJ. A developmental change in NMDA receptor-associated proteins at hippocampal synapses. J Neurosci 2000;20:1260–1271. [PubMed: 10648730]

Sans N, Racca C, Petralia RS, Wang YX, McCallum J, Wenthold RJ. Synapse-associated protein 97 selectively associates with a subset of AMPA receptors early in their biosynthetic pathway. J Neurosci 2001;21:7506–7516. [PubMed: 11567040]

Sans N, Prybylowski K, Petralia RS, Chang K, Wang YX, Racca C, Vicini S, Wenthold RJ. NMDA receptor trafficking through an interaction between PDZ proteins and the exocyst complex. Nat Cell Biol 2003;5:520–530. [PubMed: 12738960]

Sans N, Wang PY, Du Q, Petralia RS, Wang YX, Nakka S, Blumer JB, Macara IG, Wenthold RJ. mPins modulates PSD-95 and SAP102 trafficking and influences NMDA receptor surface expression. Nat Cell Biol 2005;7:1179–1190. [PubMed: 16299499]

Schluter OM, Xu W, Malenka RC. Alternative N-terminal domains of PSD-95 and SAP97 govern activity-dependent regulation of synaptic AMPA receptor function. Neuron 2006;51:99–111. [PubMed: 16815335]

Schnell E, Sizemore M, Karimzadegan S, Chen L, Bredt DS, Nicoll RA. Direct interactions between PSD-95 and stargazin control synaptic AMPA receptor number. Proc Natl Acad Sci U S A 2002;99:13902–13907. [PubMed: 12359873]

Sharma K, Fong DK, Craig AM. Postsynaptic protein mobility in dendritic spines: long-term regulation by synaptic NMDA receptor activation. Mol Cell Neurosci 2006;31:702–712. [PubMed: 16504537]

Sprague BL, McNally JG. FRAP analysis of binding: proper and fitting. Trends Cell Biol 2005;15:84–91. [PubMed: 15695095]

Star EN, Kwiatkowski DJ, Murthy VN. Rapid turnover of actin in dendritic spines and its regulation by activity. Nat Neurosci 2002;5:239–246. [PubMed: 11850630]

Stein V, House DR, Bredt DS, Nicoll RA. Postsynaptic density-95 mimics and occludes hippocampal long-term potentiation and enhances long-term depression. J Neurosci 2003;23:5503–5506. [PubMed: 12843250]

Steiner P, Higley MJ, Xu W, Czervionke BL, Malenka RC, Sabatini BL. Destabilization of the postsynaptic density by PSD-95 serine 73 phosphorylation inhibits spine growth and synaptic plasticity. Neuron 2008;60:788–802. [PubMed: 19081375]

Valtschanoff JG, Weinberg RJ. Laminar organization of the NMDA receptor complex within the postsynaptic density. J Neurosci 2001;21:1211–1217. [PubMed: 11160391]

Waites CL, Specht CG, Hartel K, Leal-Ortiz S, Genoux D, Li D, Drisdel RC, Jeyifous O, Cheyne JE, Green WN, Montgomery JM, Garner CC. Synaptic SAP97 isoforms regulate AMPA receptor dynamics and access to presynaptic glutamate. J Neurosci 2009;29:4332–4345. [PubMed: 19357261]

Washbourne P, Liu XB, Jones EG, McAllister AK. Cycling of NMDA receptors during trafficking in neurons before synapse formation. J Neurosci 2004;24:8253–8264. [PubMed: 15385609]

Xu W, Schluter OM, Steiner P, Czervionke BL, Sabatini B, Malenka RC. Molecular dissociation of the role of PSD-95 in regulating synaptic strength and LTD. Neuron 2008;57:248–262. [PubMed: 18215622]

Yi Z, Petralia RS, Fu Z, Swanwick CC, Wang YX, Prybylowski K, Sans N, Vicini S, Wenthold RJ. The role of the PDZ protein GIPC in regulating NMDA receptor trafficking. J Neurosci 2007;27:11663–11675. [PubMed: 17959809]

Yoshii A, Constantine-Paton M. BDNF induces transport of PSD-95 to dendrites through PI3K-AKT signaling after NMDA receptor activation. Nat Neurosci 2007;10:702–711. [PubMed: 17515902]

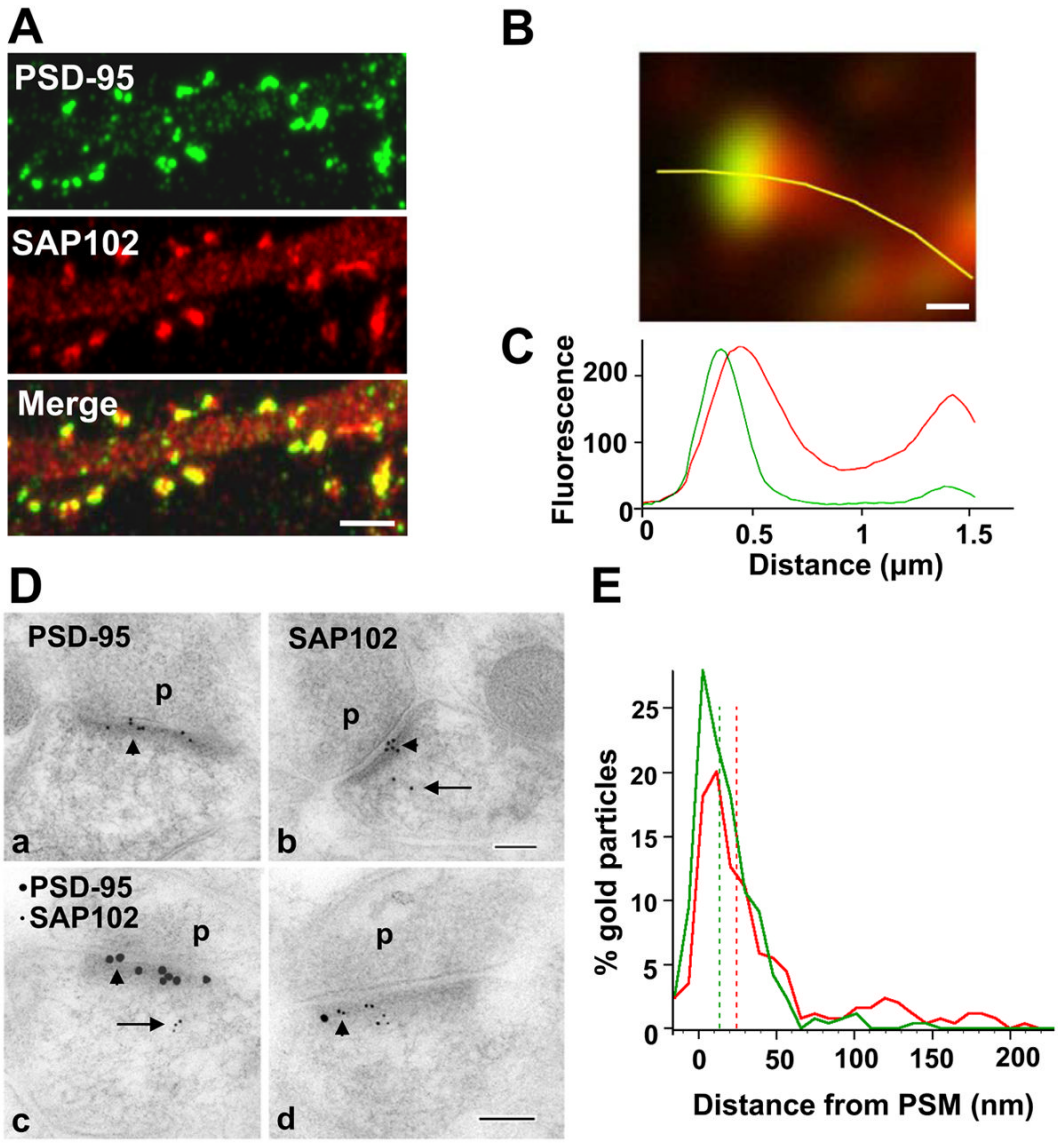

Figure 1. Distribution of SAP102 and PSD-95 in spines

A. Double staining of endogenous SAP102 (red) and PSD-95 (green) in hippocampal neurons (21 DIV). Both SAP102 and PSD-95 are enriched in spines relative to dendrites and are highly colocalized in spines but not in dendrites (more pictures in supplementary Fig. 2). Scale bar, 2 μm. **B.** High magnification image of a mushroom spine that was double stained for endogenous SAP102 (red) and PSD-95 (green). Scale bar, 200 nm. **C.** Fluorescence intensity of SAP102 (red line) and PSD-95 (green line) along the yellow marker in panel B. The X-axis shows the distance from the left end of the yellow marker, and the Y-axis is the fluorescence intensity. **D.** Immunogold labeling of SAP102 and PSD-95 in spines from CA1 stratum radiatum of the 37-day-old rat hippocampus. SAP102 is localized at the PSD (arrowhead) as well as in the cytoplasm (arrow), while PSD-95 is concentrated at the PSD (arrowhead). a, b. Single immunogold labeling of PSD-95 (a) or SAP102 (b) using 10 nm gold (2 animals for each). c, d. Sections that were double labeled for PSD-95 (15 nm gold) and SAP102 (5 nm gold) show distributions indistinguishable from those that were single labeled (2 animals). P = presynaptic terminal. Scale bar, 100 nm. **E.** Distribution of gold particles in spines from CA1 stratum radiatum of P37 rat hippocampus. There is an overlap in the localization of PSD-95

and SAP102. The median values (dash lines) are 13.5 nm from the postsynaptic membrane for PSD-95 and 24.2 nm from the postsynaptic membrane for SAP102. SAP102 is more generally distributed in the cytoplasm between 50–250 nm from the postsynaptic membrane. Data are from both single and double labeling of SAP102 or PSD-95 (n = 294 for PSD-95, including n = 192 from single labeling and n = 102 from double labeling; n = 283 for SAP102; including n = 144 from single labeling and n = 139 from double labeling). PSM = postsynaptic membrane.

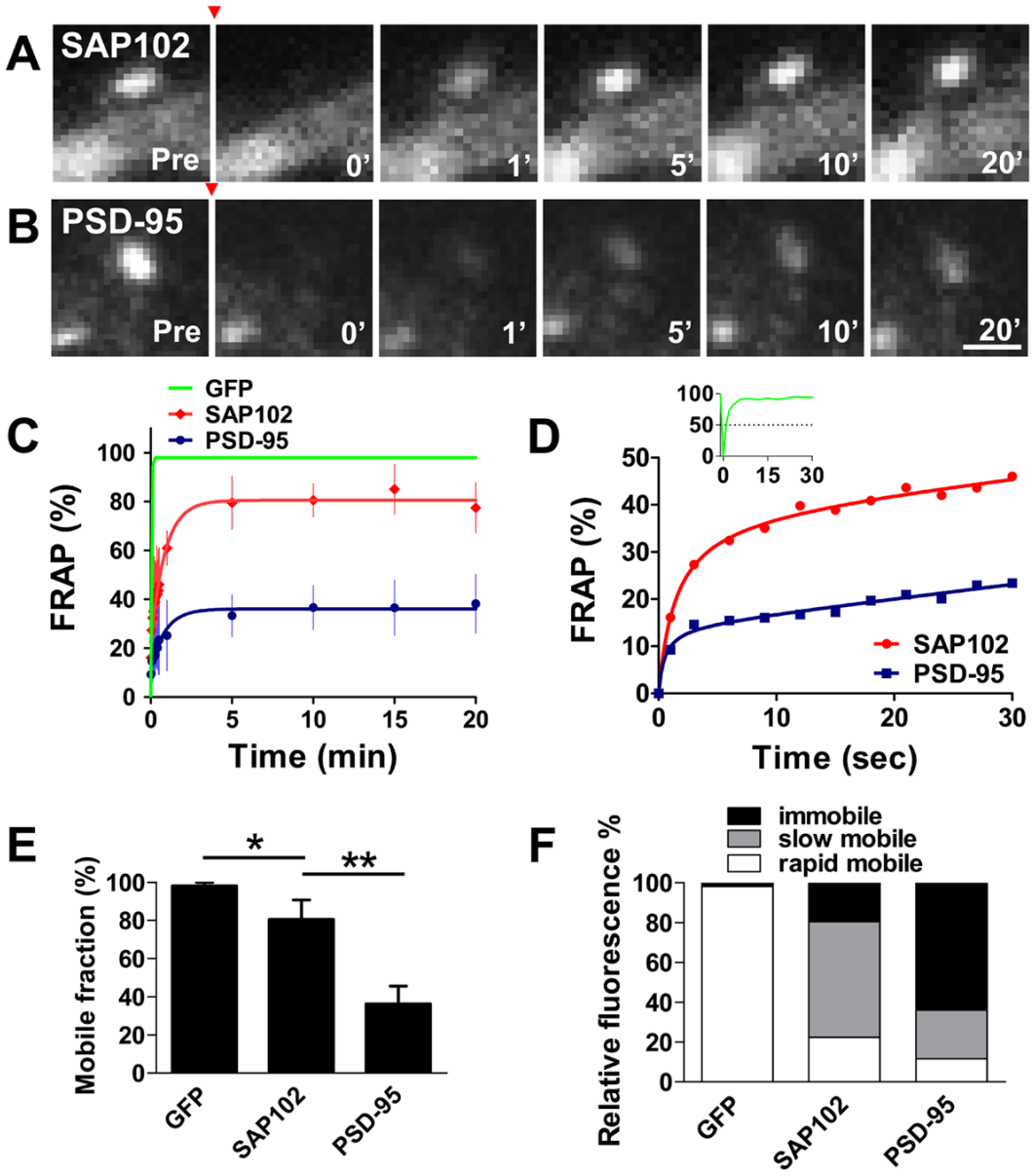

Figure 2. FRAP measurements of GFP-SAP102 and GFP-PSD-95 in spines

FRAP of GFP-SAP102 (**A**) and GFP-PSD-95 (**B**) in spines after photobleaching. The red arrowheads indicate the time of photobleaching. Photographs represent the same area before (Pre) and at 0, 1, 5, 10, and 20 minutes after photobleaching. Neurons were maintained at 37° C during the experiment. Scale bar, 1 μm. **C.** FRAP curves of GFP, GFP-SAP102 and GFP-PSD-95 in spines over a 20-minute period. The dots on GFP-SAP102 and GFP-PSD-95 curves show the FRAP every 3 seconds for the first 30 seconds, and then at 1, 5, 10, 15, 20 minutes. The curves were fit by one-phase exponential equations. The fluorescence before photobleaching was counted as 100% (n = 8, 8, and 4 for EGFP, GFP-SAP102, and GFP-PSD-95 transfected neurons, respectively). Scale bar, 1 μm. **D.** FRAP curves of GFP-SAP102 and GFP-PSD-95 over a 30-second period. The insert is the FRAP curve of GFP, showing that GFP fully recovers within 10 seconds after photobleaching. **E.** Histogram showing the mobile fraction of GFP-tagged proteins in spines. Mobile fractions of 98.2 ± 1.7% for GFP, 80.5 ± 10.2% for GFP-SAP102, and 36.2 ± 9.3% for GFP-PSD-95 were detected in 20 minutes. *p

< 0.05, **p<0.01. **F**. Histogram showing the immobile, slow mobile, and rapid mobile fractions of GFP vector, GFP-SAP102, and GFP-PSD-95 in spines, respectively. Both slow and rapid mobile fractions of GFP-SAP102 (58.1 ± 8.0%, 22.4 ± 3.7%) are larger than those of GFP-PSD-95 (24.4 ± 4.0%, 11.7 ± 3.6%).

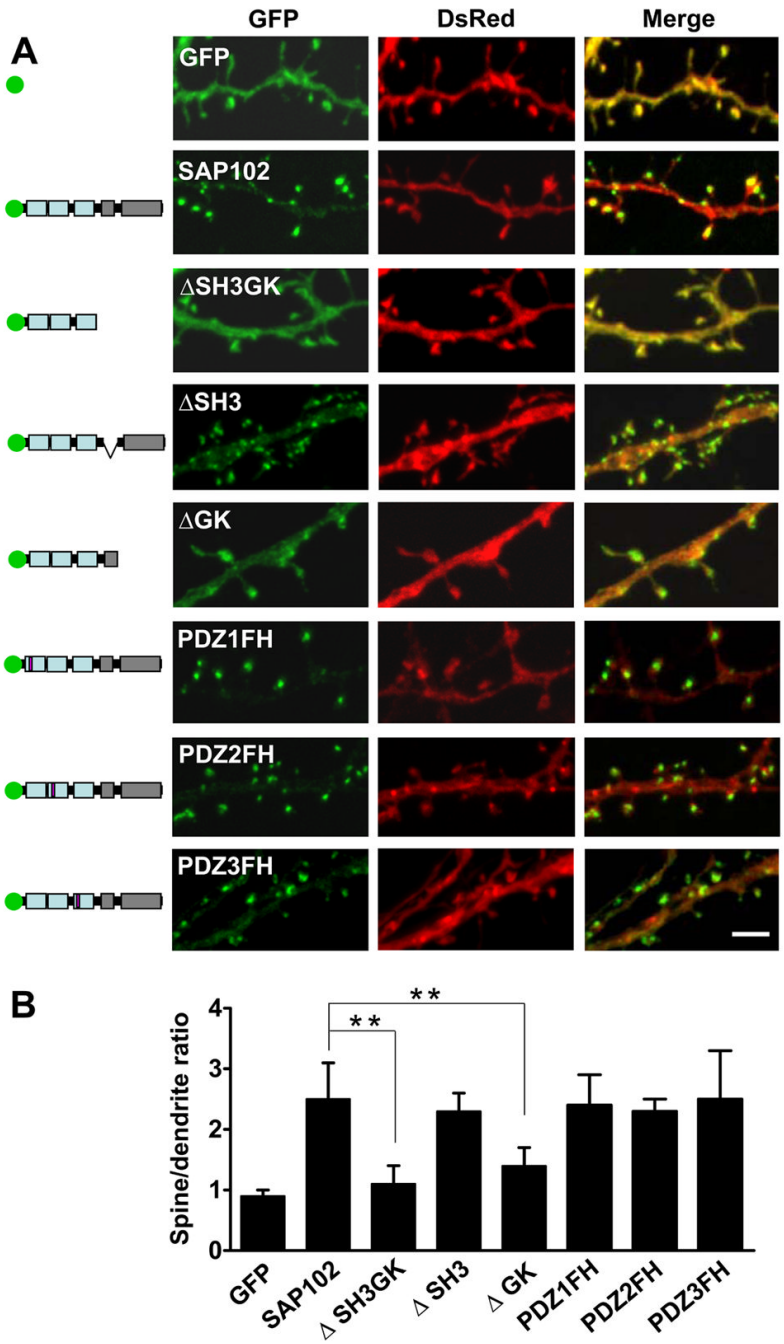

Figure 3. SH3/GK domains are necessary for SAP102 clustering in spines

A. Hippocampal neurons were co-transfected with DsRed/GFP, DsRed/GFP-SAP102, DsRed/GFP-SAP102ΔSH3GK, DsRed/GFP-SAP102ΔSH3, DsRed/GFP-SAP102ΔGK, DsRed/GFP-SAP102PDZ1FH, DsRed/GFP-SAP102PDZ2FH, or DsRed/GFP-SAP102PDZ3FH. Schematic diagrams on the left show the structure of the constructs. GFP-SAP102ΔSH3GK is uniformly distributed throughout the dendrite and the spines. GFP-SAP102ΔSH3, GFP-SAP102PDZ1FH, GFP-SAP102PDZ2FH, and GFP-SAP102PDZ3FH are enriched in spines. Scale bar, 2 μm. **B.** The mean fluorescence intensity of spines compared to that in adjacent dendrites. The spine/dendrite green fluorescence ratio of GFP-SAP102ΔSH3GK is 1.1 ± 0.3, close to the ratio of the GFP control (0.9±0.1). The ratio of GFP-SAP102ΔSH3, GFP-

SAP102PDZ1FH, GFP-SAP102PDZ2FH, and GFP-SAP102PDZ3FH are 2.4 ± 0.3, 2.4 ± 0.5, 2.3 ± 0.2 and 2.5 ± 0.8, all close to the ratio of GFP-SAP102 (2.5±0.6). n=10–15 neurons from 3 transfections. **p<0.01.

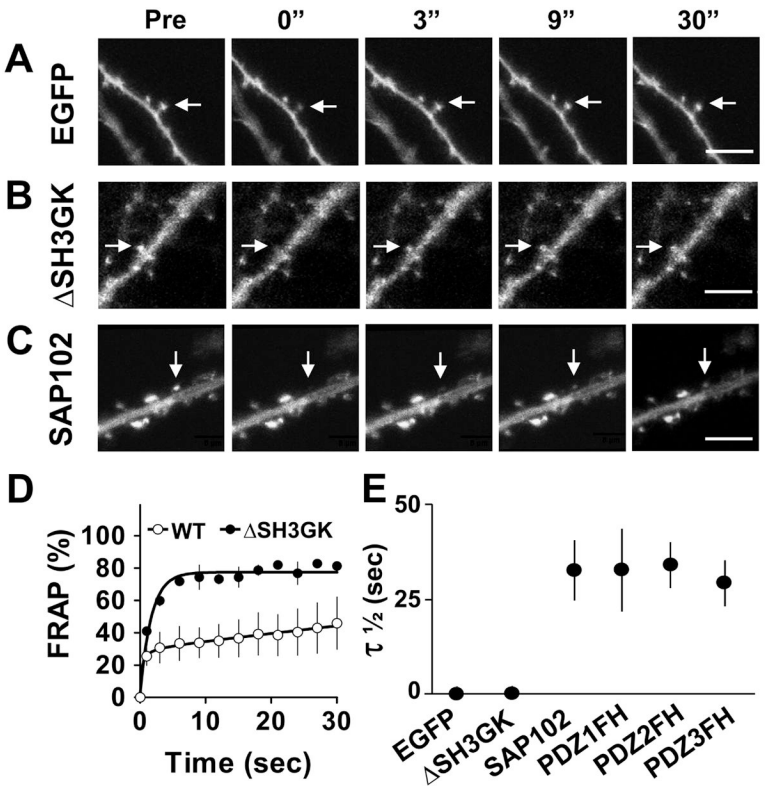

Figure 4. SH3/GK domains are necessary for SAP102 stabilization in spines

A–C. FRAP of neurons expressing GFP, GFP-SAP102ΔSH3GK or GFP-SAP102 over a 30-second period. The arrows indicate the spines of interest. Pictures were captured before (Pre) and at 0, 3, 9, and 30 seconds after photobleaching. Scale bar, 5 μm. **D.** FRAP curves of spines expressing GFP-SAP102ΔSH3GK or GFP-SAP102 over a 30-second period. N = 4 neurons, WT = wild type. **E.** Half recovery time ($\tau_{1/2}$) of GFP, GFP-SAP102ΔSH3GK, GFP-SAP102, GFP-SAP102PDZ1FH, GFP-SAP102PDZ2FH and GFP-SAP102PDZ3FH. The half recovery time of GFP-SAP102ΔSH3GK is close to that of GFP, but significantly smaller than that of GFP-SAP102, GFP-SAP102PDZ1FH, GFP-SAP102PDZ2FH and GFP-SAP102PDZ3FH. N = 4, 4, 8 neurons, **p<0.01.

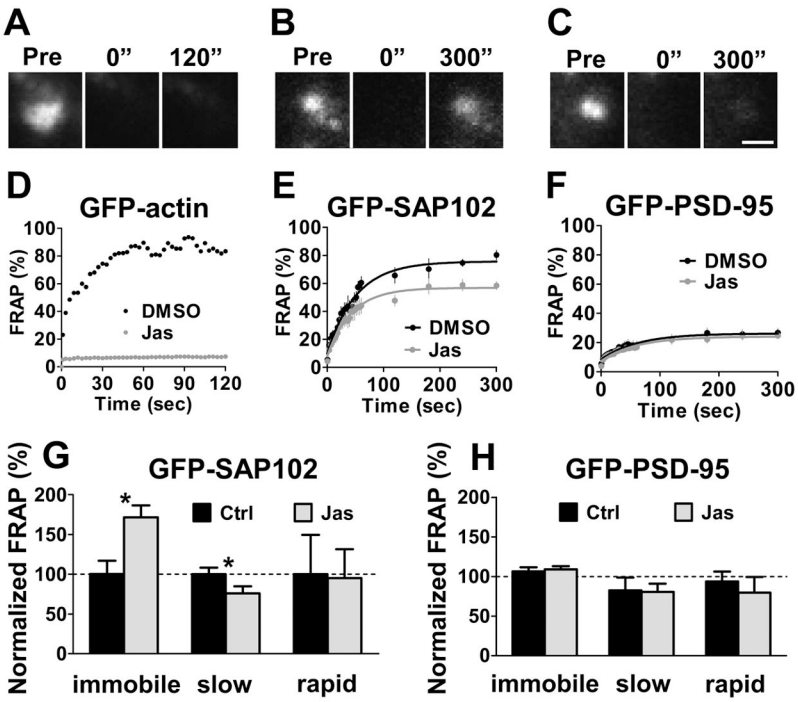

Figure 5. FRAP of GFP-SAP102 and GFP-PSD-95 in the presence of the actin stabilizer Jasplakinolide

A–C. The images represent FRAP of neurons expressing GFP-actin (**A**), GFP-SAP102 (**B**) and GFP-PSD-95 (**C**) in the presence of Jasplakinolide. The fluorescence of the same areas before (Pre) and at 0 and 120 (or 300) seconds after photobleaching are shown. Scale bar, 1 μm. **D.** FRAP sample of transfected GFP-actin in spines. The recovery was totally blocked by incubating the neurons with actin stabilizer Jasplakinolide (10 μM) for 30 minutes before FRAP measurement. The solution also contained 10 μM Jasplakinolide during imaging. Untreated cultures (black) and Jasplakinolide treated cultures (gray) are shown over a 120-second recording. Jas = Jasplakinolide. **E.** FRAP of GFP-SAP102 was partly blocked by pretreatment of Jasplakinolide for 30 minutes. N = 5 for DMSO control and n = 7 for Jasplakinolide treatment. **F.** FRAP of GFP-PSD-95 was not affected by pretreatment of Jasplakinolide. N = 8 for each. **G.** The immobile fraction of GFP-SAP102 increased and the slow mobile fractions decreased after Jasplakinolide treatment. There was no significant change for rapid mobile fractions after Jasplakinolide treatment. *$p<0.05$, Ctrl = control. **H.** There was no significant change for the immobile, slow mobile and rapid mobile fractions of GFP-PSD-95 after stabilizing actin with Jasplakinolide.

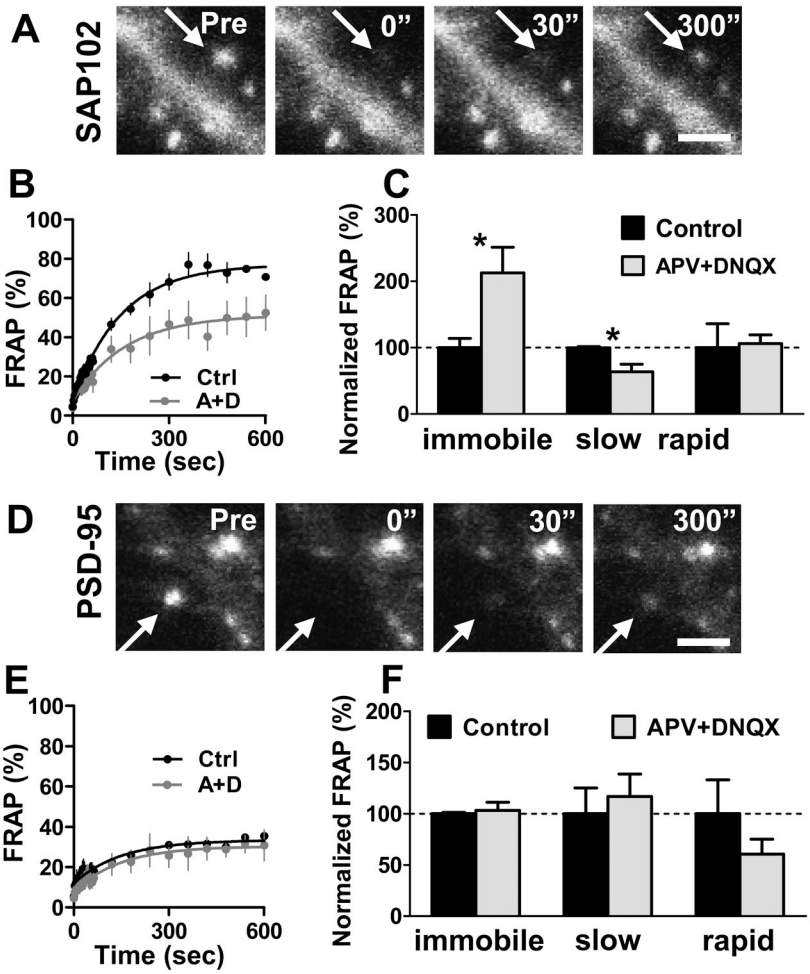

Figure 6. The mobility of GFP-SAP102 is rapid regulated by synaptic activity

A. The images represent FRAP of a neuron expressing GFP-SAP102 with blockade of NMDA and AMPA receptors. Neurons were incubated with 100 μM DL-APV and 20 μM DNQX 1 hour before experiments and during experiments. Scale bar, 2 μm. **B–C.** FRAP of GFP-SAP102 was reduced by blocking both NMDA and AMPA receptors activity. The immobile and slow mobile fractions of GFP-SAP102 decreased after APV and DNQX treatment. There was no change in rapid mobile fractions after APV and DNQX treatment. N = 4 for each FRAP curve, *$p<0.05$, Ctrl = control (black), A+D = APV+DNQX (gray). **D.** The images represent FRAP of a neuron expressing GFP-PSD-95 with blockade of NMDA and AMPA receptors. Scale bar, 1 μm. **E–F.** FRAP of GFP-PSD-95 was not affected by APV and DNQX treatment. There was no change in immobile, slow mobile and rapid mobile fractions after APV and DNQX treatment. N = 4 for each FRAP curve.